Journal of Applied Electrochemistry **30**: 61–70, 2000.

Removal of Zn(II) from chloride medium using a porous electrode: current penetration within the cathode

M.R.V. LANZA and R. BERTAZZOLI
Faculdade de Engenharia Mecânica, Universidade Estadual de Campinas, Caixa Postal 6122, 13083-970, Campinas-SP, Brazil

Received 2 February 1999; accepted in revised form 24 June 1999

Key words: current depth penetration, porous electrodes, wastewater treatment, zinc removal

Abstract

An electrolytic process for the removal of zinc from aqueous solutions using a flow-through cell with a reticulated vitreous carbon cathode is proposed. The operational conditions for the reactor were optimized as a function of the electrolyte pH, the cathode porosity and the solution flow rate. Both a synthetic solution and a real effluent from an industrial electroplating plant were processed until zinc concentration dropped from 50 to 0.1 mg dm^{-3} and from 152 to 0.5 mg dm^{-3}, respectively. After the processing of the real effluent, tomographic images of the cathode were taken in order to investigate the current depth penetration during electrolysis. Results have shown that the current density decreases from the outer surface to the centre of the RVC cathode.

1. Introduction

Aqueous effluents containing metallic ions from industrial production, processing and surface finishing of metals are conventionally treated by chemical precipitation of insoluble salts and hydroxides. For some metals, particularly zinc, conventional treatment is efficient for complying with the legislation for final discharge. The major drawback of the precipitation treatment is the sludge that remains after the separation of the solid phase.

Electrolytic cells offer an efficient means of controlling the metal ions concentration in aqueous solution via reduction reaction. Metal ions are reduced at the inner surface of porous electrodes as the electrolyte percolates through the cell. Electrolytic treatment can also be used for final polishing of the treated effluent when concentrations much less than 1 mg dm^{-3} are required prior to final discharge. The literature presents many types of electrolytic devices for the removal of metals and many case studies for the removal of different metals. All have as a goal the maximization of removal rates as a function of the electrode materials, the cathode porosity and the flow rate [1–12]. However, the effective operation of an electrochemical cell is critically dependent on the potential distribution within the porous electrode. The penetration depth of the current may be limited by ohmic losses, and the metal deposition may occur via a process not fully mass transfer controlled.

Zinc is widely employed as a protective coating onto ferrous materials, and electrolytic deposition from an acidic plating bath is the most common process [13]. As the main consumer of metallic zinc and its compounds, the electroplating industry is a source of Zn(II)-containing aqueous waste. Drag-out from plating baths is responsible for the zinc ion concentration in the rinse water continuously discharged into the effluent treatment unit. Selective separation and recovery of zinc from aqueous ternary mixtures of metals has been reported [14], but the deposition of metals was, apparently, not mass-transfer controlled, pointing to the conclusion that rates of removal are electrode porosity and flow rate independent. A rotating cylinder smooth electrode reactor has been used for zinc recovery from aqueous mine residue [15] where small amounts of synthetic and process sulphate solutions of low pH, were processed and exhibited low current efficiency when electrolysis was carried out under mass transfer control.

Zinc ions have low toxicity and the legislation adopted in many countries demands 5 mg dm^{-3} of Zn(II) containing solution for final discharge of the aqueous waste stream [16]. However, a medium sized automatic industrial plant of zinc plating may discharge up to 1000 dm^3 $h^{-1}$of rinse water with Zn(II) concentration ranging from 40 to 200 mg dm^{-3}. Here we investigate the performance of a flow-through cell, with a reticulated vitreous carbon cathode (RVC), for the removal of zinc taking into account that the mass of zinc to be chemically precipitated from the aqueous waste streams is responsible for the generation of a large amount of sludge. First, a study of the influence of pH of the medium on the zinc deposition was conducted. Then, using a synthetic solution, the influence of the

cathode porosity and flow rate on the removal rate was investigated. Following this study, a new series of experiments was carried out using a real effluent from the first rinse water tank from an automated zinc plating industrial plant. Tomographic images of the cathode allowed for an estimation of the current penetration depth during electrolytic zinc removal. The reasons for the choice of RVC as a cathode material are summarised elsewhere [17].

2. Experimental details

Initially, a voltammetric study of the Zn(II) reduction reaction on a glassy carbon rotating disc electrode was performed to determine the range of potentials over which this reaction is controlled by mass-transfer and the dependence of these potentials on pH. Then a value of potential within this range was selected and applied to a flow-through electrolytic cell.

All electrochemical experiments were performed using a model 273A potentiostat/galvanostat system controlled by the software model 270/250 (both from EG&G Princeton Applied Research Corp.). A model 3110 Perkin Elmer spectrometer was employed to determine the Zn(II) concentration, using an air/acetylene flame. After completing the experiments using real effluent, the cathode was examined by X-ray tomography using General Electric, model 9800, equipment. Tomographic data were taken using X-rays of 120 kV, current of 70 mA in the filament, and the data were recorded as a 512×512 square matrix. Changes of density detected within the electrode permitted the quantification of the mass of deposited zinc. Then, Faraday's law was used to estimate the current within each 1.5 mm thick tomographic slice of the 12 mm thick RVC cathode.

In the first part of this study, using synthetic effluent, all reagents were of analytical grade and solutions were prepared using distilled and deionised water. The Zn(II) solution was prepared from $ZnCl_2$ (50 mg $dm^{-3}$of Zn(II)) using boric acid (0.1 M) plus potassium chloride (0.1 M) as the supporting electrolyte. HCl solution or KOH solution was used to adjust the pH to the required value. The pH of the solutions used in the experiments was increased from 2.5 to 5.5 in increments of 0.5. For the study using real effluent, a 152 g dm^{-3} zinc solution with a pH of 5.5, was supplied by Freios Varga S.A.

A glassy carbon rotating disc electrode (GCRDE) model 616 (PARC) was used as a working electrode ($A = 0.12$ cm^{-2}) in the hydrodynamic voltammetric experiments. A platinum counter-electrode and a saturated calomel reference electrode (SCE) with a Luggin capillary were also used. The voltammograms were obtained in 50 mg dm^{-3} Zn(II) solutions for several rotation rates (41.9, 94.2, 167.5, 261.8 and 376.9 rad s^{-1}) by cycling the working electrode potential (one cycle) between -0.20 V and -1.60 V at 5 mV s^{-1}.

The continuous-flow circuit and the flow-through cell have been previously described [12], and the RVC sponges were supplied by the Electrosynthesis Co.

After assembling the electrochemical cell, the flow system was loaded with 3.5 dm^3 of catholyte and anolyte, each in a separate reservoir. The synthetic catholyte consisted of the Zn(II) solution described above. The real catholyte was a solution with unknown concentrations of boric acid and potassium chloride, traces of organics used as levelling, wetting and brightening agents, and 152 mg dm^{-3} of Zn(II). This 5.5 pH solution had a conductivity three times lower than the synthetic solution. The anolyte composition was the same as the synthetic catholyte, but without Zn(II). At predetermined intervals, the solution leaving the cathodic compartment was sampled, and the remaining Zn(II) concentration was quantified by atomic absorption spectrometry to monitor the effectiveness of electrolysis. The above procedure was used to examine the efficiency of RVC cathodes of different porosities (45, 60, 80 and 100 ppi) and different flow rates for the synthetic catholyte. For the real effluent only an 80 ppi RVC was used at a flow rate of 120 dm^3 h^{-1}.

3. Results and discussion

3.1. *Preliminary hydrodynamic voltammetric experiments*

Figure 1 shows i/E curves recorded in the hydrodynamic mode for the synthetic Zn(II) solution of pH 5.5. As stated earlier pH was increased from 2.5 to 5.5 in increments of 0.5 and, due to the similarity between the series of voltammograms, Figure 1 presents results recorded for pH 5.5. In the forward scans all the curves show waves for the reduction of Zn(II) to Zn, with a well-defined limiting current plateau extending over a potential range of at least 250 mV. The value of the limiting current was dependent on the GCRDE rotation rate. This behaviour is characteristic of a mass-transfer controlled process. In the cathodic region of the reverse scan, the current magnitude over the limiting current plateaux was higher than that registered in the forward scan. This feature is to be expected for a system involving nucleation and growth of a metal phase on the carbon electrode. In the reverse sweep, an oxidation peak current was also observed at -1.1 V for all voltammograms. All features described above are absolutely extensive to the curves obtained for all values of pH, except for the values of the limiting currents and for the positioning of cathodic events on the potential axis.

Figure 2 shows Levich plots, for the limiting currents measured at the mid point of the plateau (-1.4 V vs SCE) plotted as a function of the square root of rotation rate ($I/f^{1/2}$), for the pH values considered in this study. The plots were linear, confirming that zinc deposition was mass-transport controlled at the potentials consid-

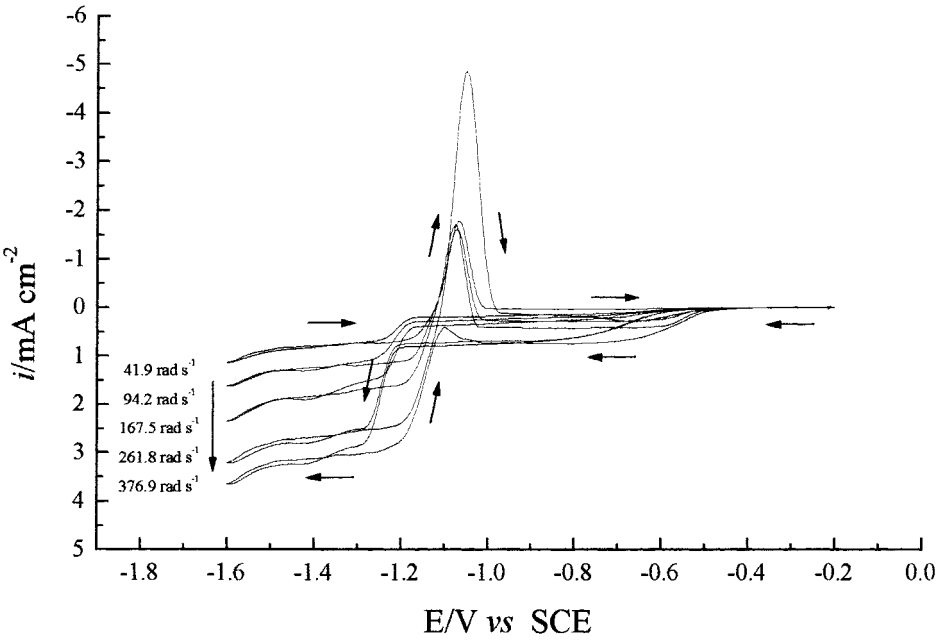

Fig. 1. Voltammograms obtained on a glassy carbon rotating disc electrode. Solution of 50 mg dm^{-3} of Zn(II) in 0.1 M of boric acid and 0.1 M potassium chloride at pH 5.5. Potential scan rate of 20 mV s^{-1}. Angular velocity as indicated on the graph.

ered. For lower values of pH the limiting currents are higher. As the pH increases, a decrease is observed in the limiting currents with a clear tendency to become constant from pH 4. From pH 4 the straight lines in the Levich plots are superimposed. The inset in Figure 2 shows a plot of the slopes taken from the straight lines in the Levich plots as a function of pH. As a result of the superimposition of the curves from Figure 2, Levich slopes became constant in the pH range 4 to 5.5 in which zinc deposition is apparently pH independent. Reduction in the limiting currents as pH increases may be due to the decrease in the hydrogen evolution currents. Proton reduction is always the unavoidable competitive parallel process to zinc deposition [18–21] and the charge imbalance in the voltammograms from Figure 1 is evidence of this fact.

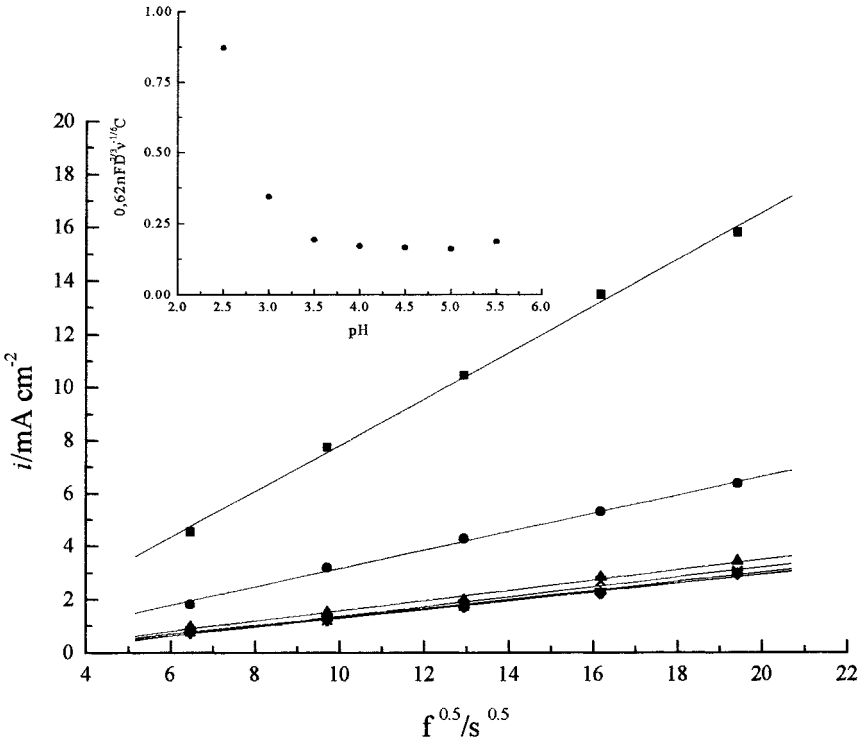

Fig. 2. Levich plots using the limiting current values taken at −1.4 V vs SCE for the solutions with pH as follows: (■) 2.5, (●) 3.0, (▲) 3.5, (▼) 4.0, (◆) 4.5, (+) 5.0 and (×) 5.5. Inset: Slopes of the Levich's plot against pH.

Although the Levich plot is an appropriate tool to verify whether an electrochemical process is mass transfer controlled or not, in this case zinc deposition became diffusion controlled at different values of potential, depending on the pH of the solution. The limiting current plateau became well defined at more positive potentials as pH increased. The shifting of potentials to more positive values as pH increases is shown in Figure 3 which depicts the variation of the potentials from which zinc deposition became diffusion controlled (E_{PLAT}) and the variation of the half wave potentials ($E_{1/2}$) with the pH. Again pH 4 is the value from which zinc deposition starts to be reproducible, and both potentials, E_{PLAT} and $E_{1/2}$ become constant.

The shifting of potentials to more positive values for higher pH makes the zinc reduction easier. This is not the expected behaviour for the critical values of potential of a redox couple. However, zinc reduction exhibits a complex mechanism and investigations of electrocrystallisation of zinc have been reported in the literature [22–26]. Particularly interesting is the series of studies carried out by Epelboin and co-workers [23–25] featuring a complex multistage stepped mechanism involving Zn^{2+}, Zn^{+}, H^{+} species, anion adsorption and intermediates adsorption. The seven equilibria, proposed as intermediate steps for the whole deposition reaction, are critically pH and potential dependent. The concurrence of all half reactions or some of them depends on the pH of the solution and of the reducing potential.

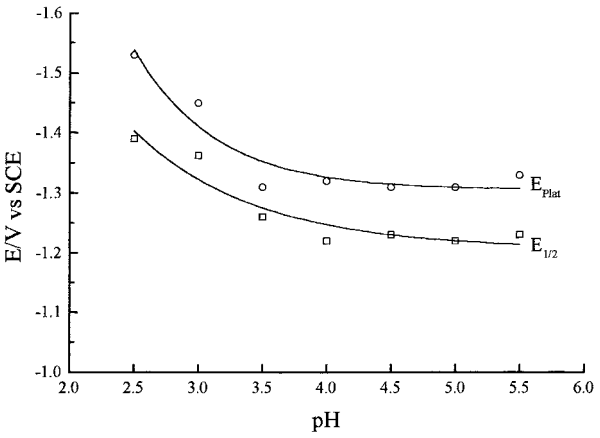

Fig. 3. Shifting of the half wave potential ($E_{1/2}$) and of the potentials in which zinc deposition becomes mass transfer controlled (E_{Plat}) to a more positive values as the solution pH increases.

Results obtained for the cyclic voltammetry on rotating glassy carbon electrodes are a good indication of the range of pH in which zinc reduction under mass transfer control is reproducible and in which zinc removal experiments can be carried out.

Fortunately, real ion zinc effluents have a pH between 5 and 6, which makes the removal operation feasible. A similar voltammetric study was also performed using the 152 mg dm^{-3} of zinc real effluent, pH 5.5. Figure 4 shows the cathodic portion of the i/E curves recorded on vitreous carbon in the same conditions described above for the synthetic solution. Current density plateaux can be observed in the same range of potentials. Besides the differences in composition, conductivity and zinc concentration, the potential of -1.4 V is an appropriate potential to conduct the experiments for both the synthetic and real solution.

3.2. *Flow-through cell performance in zinc removal from synthetic solution*

In flow-through cell performance studies, the removal of Zn(II) was conducted in the batch recirculation mode. In

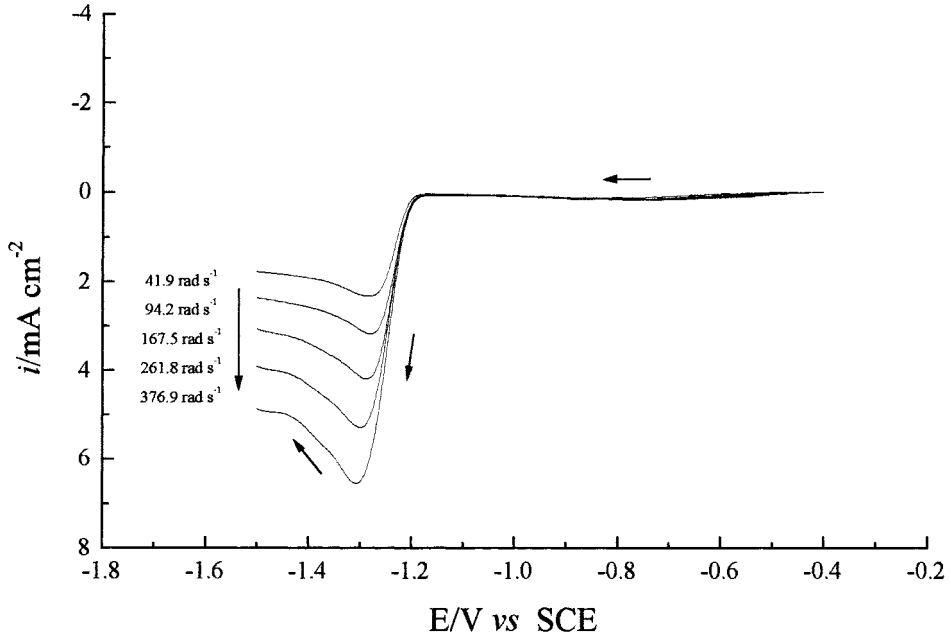

Fig. 4. Voltammograms of Zn(II) reduction in the real effluent on a glassy carbon rotating disc electrode. Zn(II) concentration of 152 mg dm^{-3}. Angular velocity as indicated on the graph and potential scan rate of 20 mV s^{-1}.

the first experiments solutions containing zinc ions with initial pH of 2.5, 4.0 and 5.5 were used. Considering the results previously obtained for lead removal [12], the electrolysis was carried out using a 80 ppi cathode and a flow rate of 120 $dm^3\ h^{-1}$. Figure 5 shows the plot of normalized concentration ($C(t)/C(0)$) as a function of recirculation time. Again the influence of pH on the zinc reduction is apparent. An improvement in cell performance is observed as the initial pH increases. Curves obtained from pH 4 are superimposed, a value from which the cell performance is reproducible. After electrolysis was terminated, the final pH was about 8 in all experiments.

Exponential decay of metal concentration is only observed if the reduction reaction occurs at limiting current [9]. Therefore, an applied potential of −1.4 V apparently causes the reaction within the porous cathode to be mass transfer limited. Figure 5 also shows, in the inset, a plot of $\ln[C(t)/C(0)]$ against time. Although the plots of $C(t)/C(0)$ as a function of electrolysis time were apparently exponential, the expectation of linearity for the $\ln[C(t)/C(0)]$ against time plot was confirmed only for a portion of the curve, as observed earlier [12]. Restricting the analysis to 30 min of electrolysis (5 to 35 min), slopes (s) from straight lines in the plot of $\ln [C(t)/C(0)]$ against time give an indication of the cell performance, since they are related to the mass transfer coefficient. A model of concentration–time relationships in recirculating electrochemical reactor systems has been proposed by Walker and Wragg [27]. An approximate solution arose from this study in which the slope (s) in the plot of $\ln[C(t)/C(0)]$ against time is

$$s = \frac{1 - \exp\left[-\frac{k_m A_e V_e}{Q}\right]}{\tau} \tag{1}$$

where V_e is the cathode volume, Q is the catholyte flow rate, A_e is the specific surface area (the active area/unit volume of cathode), k_m is the mass transfer coefficient and τ is the residence time. Expanding the argument of the exponential function in a Taylor series and taking the two first terms, $1 - \exp(-x) \simeq x$ for low values of x, and Equation 1 becomes:

$$s = \frac{V_e}{V} k_m A_e \tag{2}$$

in which τ was replaced by V/Q and V is the total volume of catholyte. Considering the ratio $V_e/V = 0.027$ used in these experiments and the values of $k_m A_e$ depicted in Table 1, the error by using Equation 2 rather than Equation 1 is around 0.2%, so that Equation 2 was used for the $k_m A_e$ estimation. Table 1

Table 1. Initial Zn(II) concentrations for each experiment at pH shown, the electrolysis times for 90% concentration reduction and values of $k_m A_e$

pH	$C(0)$/mg dm^{-3}	$t_{90\%}$/s	$k_m A_e/s^{-1}$
2.5	60.2	1380	0.124
4.0	54.8	960	0.148
5.5	54.4	960	0.148

Flow rate of 120 $dm^3\ h^{-1}$ and cathode porosiy of 80 ppi

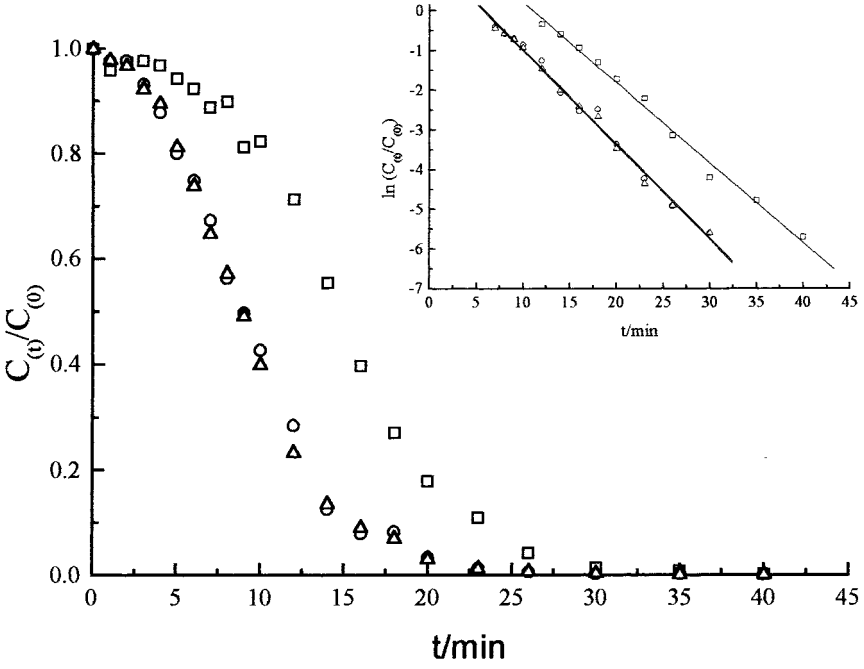

Fig. 5. Normalized concentration $[C(t)/C(0)]$ against time curves for zinc removal experiments for different pH values, obtained for a 120 $dm^3\ h^{-1}$ flow rate and cathode porosity 80 ppi. The pH values are as follows: (□) 2.5, (○) 4.0 and (△) 5.5. Inset: Plots of $\ln [C(t)/C(0)]$ against time for the data shown.

shows values of initial concentrations, $C(0)$, the times for 90% removal, $t_{90\%}$, and values of k_mA_e as a function of pH. Data show that the mass transfer coefficient increases with pH and becomes constant from pH 4.

The experiments depicted in Figure 5 were never terminated before zinc concentration in the electrolyte reached 0.5 mg dm^{-3}. Moreover, as expected for a constant potential bulk electrolysis under mass transfer control, the time for 99% zinc reduction is around twice the times shown in Table 1, for 90% reduction.

In view of the findings for different pH, solutions of pH 5.5 were selected for the new series of experiments in which the influence of flow rate and cathode porosity on cell performance were investigated. Figure 6 shows the curves of normalized concentration as a function of time using four values of cathode porosity, where electrolysis was carried out at a flow rate of 120 dm^3 h^{-1}. As expected, an exponential decay of zinc concentration is observed. Figure 6 also shows the $\ln[C(t)/C(0)]$ against time plot for 30 min electrolysis following the earlier procedure. From Figure 6 it is possible to see that cathode porosity can be used for the optimization of cell performance, which is in agreement with literature data [2–12]. Table 2 shows the effect of cathode porosity on the removal rate of zinc and on the values of k_mA_e, calculated from the linearization shown in the inset of Figure 6.

Most of the improvement observed in the cell performance is due to the increase in the available specific surface area for the reaction since RVC is a poor turbulence promoter. However, for the porosity of 100 ppi no improvement in the mass transfer coefficient was observed. For higher porosity RVC sponges, the manufacturer's literature shows an overlap of the porosity range for porosity grades of 80 and 100 ppi (±(10–20)% of variation of nominal values), which can make the surface area of the cathodes close enough to make the data indistinguishable.

Table 2. Effect of the RVC cathode porosity on the removal rate of zinc from chloride medium, pH 5.5

Porosity/ppi	$C(0)$/mg dm^{-3}	$t_{90\%}$/s	k_mA_e/s^{-1}
45	59.6	2400	0.068
60	54.4	1500	0.111
80	54.4	960	0.145
100	54.1	1020	0.136

Flow rate of 120 dm^3 h^{-1}

Using a sponge with porosity of 80 ppi and flow rate of 120 dm^3 h^{-1}, a concentration of 0.5 mg dm^{-3} was reached in 15 min and a final concentration of 0.1 mg dm^{-3} required 25 min electrolysis. This performance can be further improved by using higher flow rates. The influence of electrolyte flow rate on the effectiveness of electrolysis is depicted in Figure 7, which shows the normalized concentration decay as a function of time and the linearised concentration profile (see the inset). The data show that, using an 80 ppi sponge, as the flow rate increases the reduction of Zn(II) becomes more effective. Following the same procedure described above, values of k_mA_e were calculated from the slopes of the $\ln[C(t)/C(0)]$ against t plot for each flow rate considered. These values are depicted in Table 3 which also shows initial concentrations for each experiment

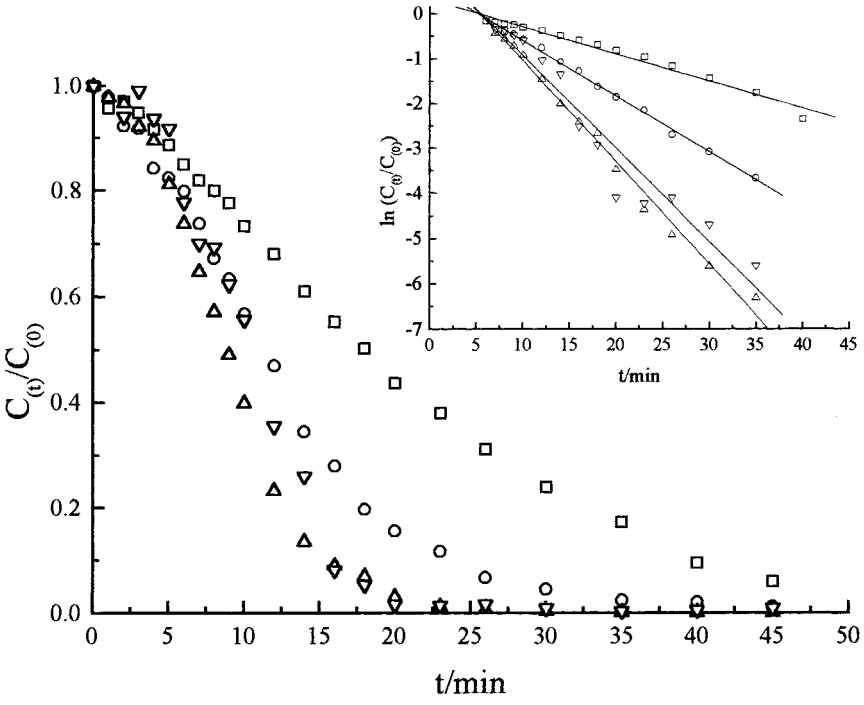

Fig. 6. Normalized concentration $[(C(t)/C(0)]$ against time curves for zinc removal experiments for different cathode porosities, obtained for a 120 dm^3 h^{-1} flow rate and pH 5.5. Porosities are as follows: (□) 45, (○) 60, (△) 80 and (▽) 100 ppi. Inset: Plots of $\ln[C(t)/C(0)]$ against time for the data shown.

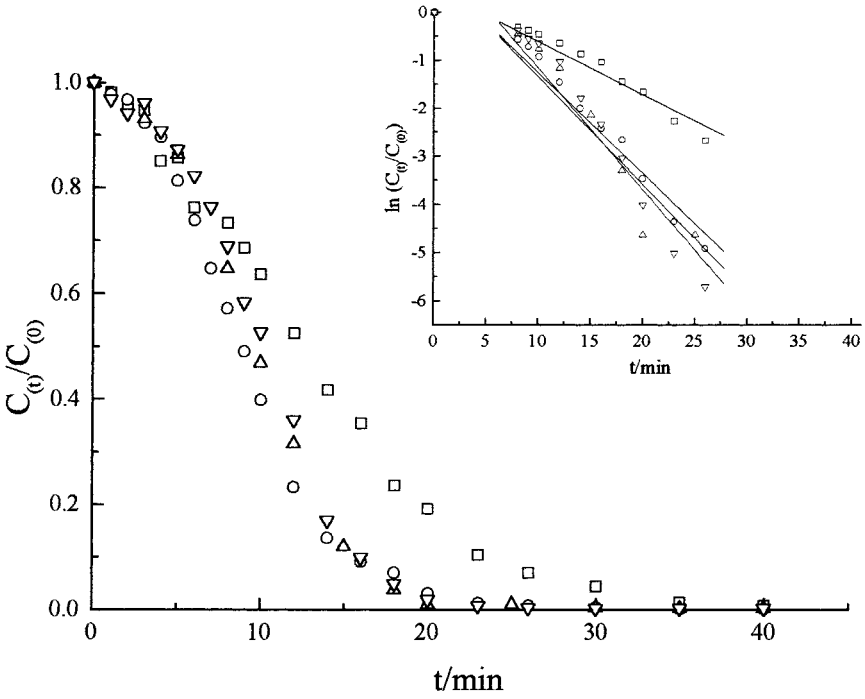

Fig. 7. Normalized concentration $[(C(t)/C(0)]$ against time curves for zinc removal experiments for different flow rates, obtained for pH 5.5 and cathode porosity 80 ppi. Flow rates are as follows: (□) 40, (○) 120, (△) 160 and (▽) 320 $dm^3\ h^{-1}$. Inset: Plots of $\ln[C(t)/C(0)]$ against time for the data shown.

and the time demanded for 90% reduction in Zn(II) concentration.

3.3. *Electrolytic removal of zinc from the real effluent*

Taking the results obtained for the synthetic effluent into account, the real effluent was processed using an 80 ppi cathode and a flow rate of 120 $dm^3\ h^{-1}$. At −1.4 V vs SCE (value taken from Figure 4) the initial zinc concentration of 152 mg dm^{-3} dropped to 10% from the initial value in 80 min and reached 1 mg dm^{-3} in 110 min. Figure 8 shows the decay of the Zn(II) normalized concentration as a function of recirculation time. The profile of the concentration decay is different from that expected. On the basis of the observed behaviour, it was hypothesized that the reduction reaction was not fully mass transfer controlled within the porous electrode. In order to investigate this hypothesis a tomographic analysis was carried out within the electrode. The decay of X-ray intensity passing through the electrode was recorded. Cumulative intensity decay caused by the crossing of n voxels (volume elements) are organized in a square matrix and transformed into the tomographic image. This matrix is considered as a pseudo-density map where each voxel presents a numerical attribute called a Hounsfield unity (H) which is proportional to the density of the material. Planes 1.5 mm thick were examined, and the mass of reduced zinc was quantified considering that the variation of each tomographic coefficient unit ($1H$) corresponds to a density variation of 2.5 mg cm^{-3} [28]. The values of H were measured by the equipment considering the difference between light and dark regions. Then, tomographic images were constructed using Khoros software.

Table 3. Effect of the flow rate on the removal rate of zinc from chloride medium, pH 5.5

Flow rate/$dm^3\ h^{-1}$	$C(0)$/mg dm^{-3}	$t_{90\%}$/s	$k_m A_e/s^{-1}$
40	55.4	1380	0.085
120	54.4	960	0.145
160	51.4	910	0.154
320	48.3	840	0.188

Cathode porosity of 80 ppi

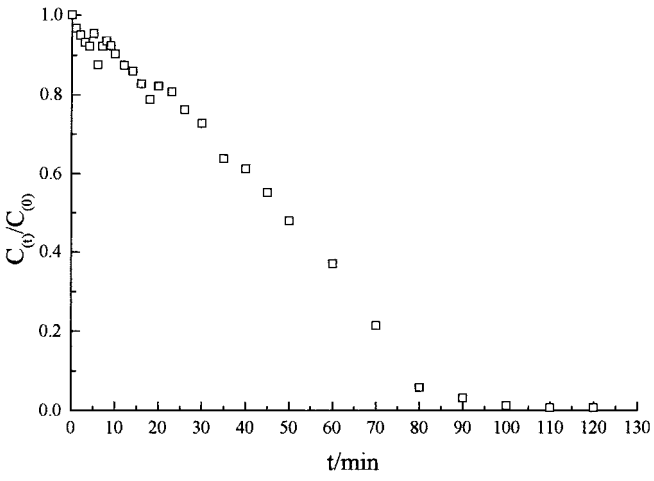

Fig. 8. Normalized concentration $[(C(t)/C(0)]$ against time curves for zinc removal experiments for the real effluent, obtained for a 120 $dm^3\ h^{-1}$ flow rate, pH 5.5 and cathode porosity 80 ppi.

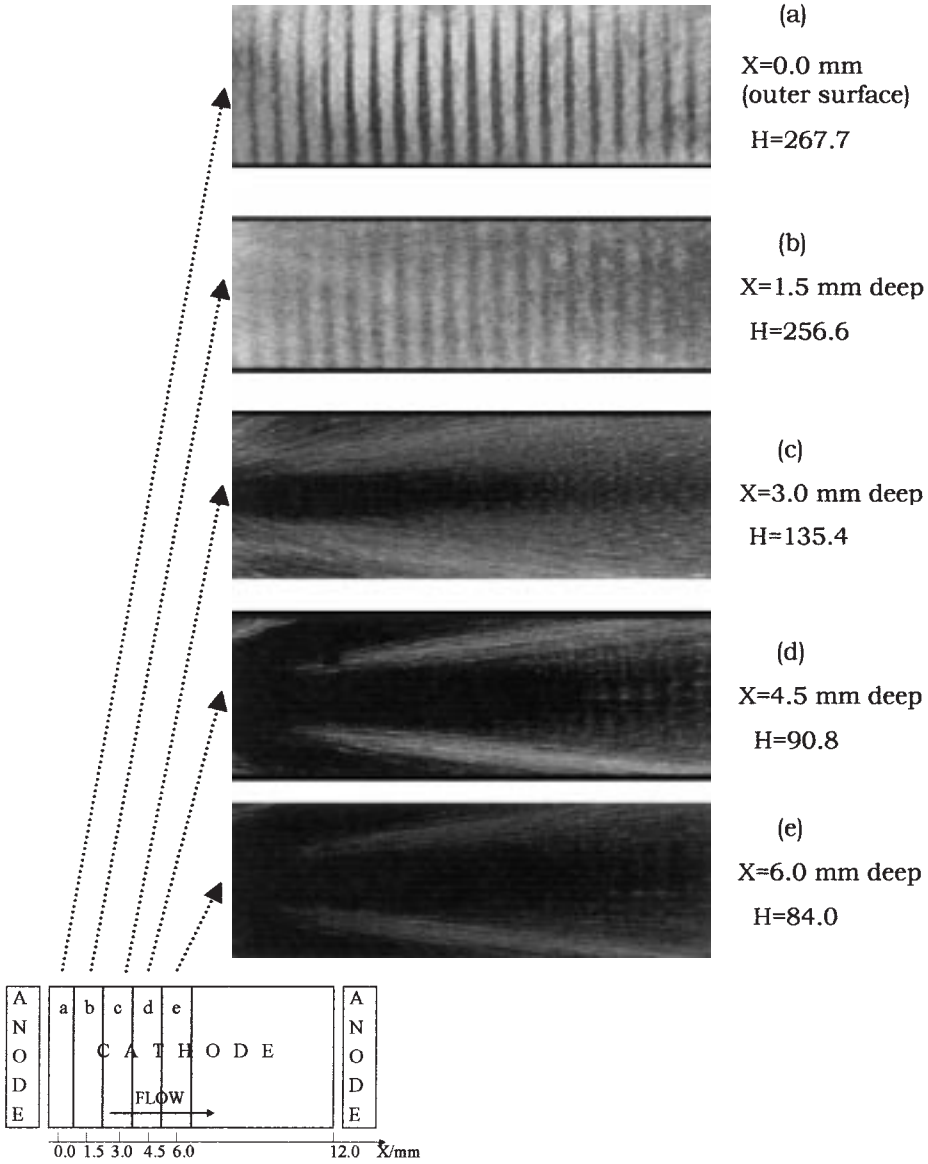

Fig. 9. RVC electrode tomographic images with zinc deposit taken each 1.5 mm deep. Values of Hounsfield coefficient (H) are shown.

Figure 9 shows images of the 'sliced' cathode. Figure 9(a) is the outer surface of the RVC electrode after the electrolysis has been terminated and the parallel marks are due to the turbulence promoter that is placed very close to the cathode. Figure 9(b)–(e) are images of zinc deposited within the electrode. Comparison between light and dark regions shows that mass of zinc decreases from the outer surface to the centre of the electrode. As described in the experimental section, the cell consisted of a 12 mm thick RVC cathode sided by two flat anodes, in such a way that Figure 9 presents images of the first half. Values of H for the second half are very close to those shown in the Figure.

From the images shown in Figure 9, the mass of deposited zinc was estimated taking into account the values of H and their relationship with the changing density. The value of H found for the clean surface ($H = 73.7$) was subtracted from the values found for each slice. The variation of H, or ΔH, represents the attenuation of the radiation due to the mass of deposited zinc. The mass of zinc inside a tomographic slice was calculated using Equation (2):

$$m_{Zn} = \Delta H \times 2.5 \times 10^{-3} \times t\, A_e(1 - v) \qquad (3)$$

where t is the thickness of the tomographic slice (1.5 mm), A is the specific surface area of the electrode and v is the voidage of the RVC cathode. According to the manufacturer's literature, A_e is 55.8 cm^2 cm^{-3}, for 80 ppi sponge, and v is 0.97. The mass of zinc contained inside each slice was related to current density values using Faraday's law. Figure 10 shows the values of current density within the sponge. The symmetry is due to the positioning of the current feeder at the centre of the electrode ($x = 6.0$ mm in the Figure 10) which is sided by two flat anodes. Figure 10 also shows that the density current is constant only in the first 1.5 mm on both sides, decreasing from the outer surface to the

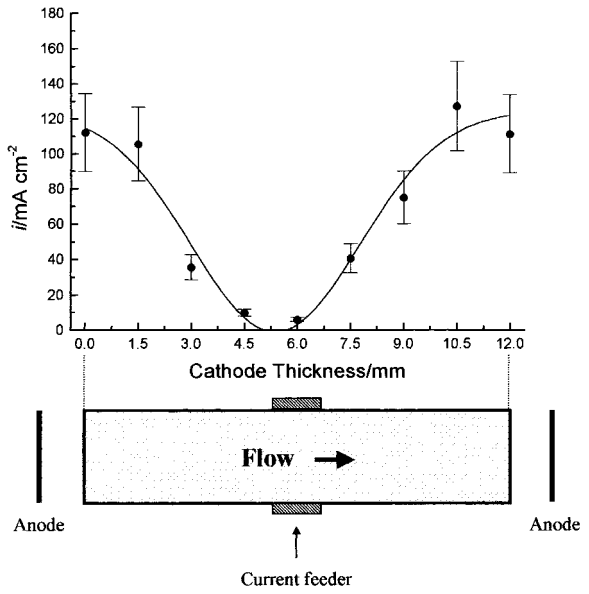

Fig. 10. Current density depth penetration profile within the porous electrode.

centre, where almost no zinc deposit was found. A similar profile of zinc distribution (apparent zinc density variation) within RVC foams was also found by Iacovangelo and Will [29] during zinc deposition in a flow-by cell configuration under charge-transfer control. Using the densitometry technique in X-ray radiograph film negatives, the distribution of zinc was found to be flow rate dependent and foam thickness and porosity dependent.

Considering the cell $k_m A_e$ value of 0.145 s^{-1} (80 ppi sponge porosity and 120 dm^3 h^{-1}) previously calculated in Table 2, and the literature formula [30, 31], the ideal thickness for this sponge would be 3.2 mm and the experiments have shown that 1.5 mm is the deepest that limiting current can reach. For thin electrodes with high conductivity electrolytes the established theoretical treatment is adequate [30]. However, the assumption of fully mass transfer controlled metal deposition, a high conductivity electrolyte and the fully conductive electrode material lead to an overestimation of the calculated value in many cases. In this study the calculated ideal thickness is twice the observed value. Ohmic losses within porous electrodes may change a mass-transfer limited operation to a mixed controlled process, where electron transfer may play an important role. The reasons may be the electrolyte conductivity, the electrode conductivity or even the physical distance between cathode and counter electrode. In the case of this study the reason is probably the difference in conductivity between the electrolytes since we used the same cell design and the same electrode material. The real effluent had lower conductivity in comparison with the synthetic one, which caused an increase in the iR drop within the cell. Synthetic effluent had a conductivity of 13 mS, three times greater than the conductivity of the real effluent.

A similar profile for the current density distribution within a porous electrode, shown in Figure 10, has been theoretically predicted. Doherty and coworkers [32] presented a model that simulates the distribution of potential and current density within a porous electrode. The model includes consideration of the electron transfer control regime of the electrode reaction, mass transport limitations and the finite conductivity of the electrode material. Simulated results are presented for several values of electrolyte conductivity, and the plots of current depth penetration are similar to that found experimentally in this work.

4. Conclusions

Hydrodynamic voltammetry was used for the determination of the range of potential over which Zn(II) reduction is mass-transfer controlled. Using these potentials in the porous electrode cell, the concentration of the metal ion in the synthetic solution was reduced from 50 to 0.1 mg dm^{-3} during recirculation times ranging from 20 to 40 min, depending on the RVC porosity, flow rate and pH.

In experiments using real effluent, for the chosen cell design and for the composition of the effluent used, zinc removal was under mass transfer control in the first 1.5 mm of the electrode. For deeper positions within the cathode the reduction reaction was under mixed control, where electron transfer also played an important role in controlling the reaction rate. This could be an effect of the poorer conductivity of the electrolyte.

The cell design used in this study showed a good performance for the removal of zinc from simulated and real effluent.

References

1. R. Alkire and P.K. Ng, *J. Electrochem. Soc.* **124** (1977) 1220.
2. A. Tentorio and U. Casolo-Ginelli, *J. Appl. Electrochem.* **8** (1978) 195.
3. R.E. Sioda and H. Piotrowska, *Electrochim. Acta* **25** (1980) 331.
4. Y. Oren and A. Soffer, *Electrochim. Acta* **28** (1983) 1649.
5. D. Simonssom, *J. Appl. Electrochem.* **14** (1984) 595.
6. M. Matlosz and J. Newman, *J. Electrochem. Soc.* **133** (1986) 1850.
7. S. Langlois, J.O. Nanzer and F. Coeuret, *J. Appl. Electrochem.* **19** (1989) 736.
8. R. Carta, S. Palmas, A.M. Polcaro and G. Tola, *J. Appl. Electrochem.* **21** (1991) 793.
9. D. Pletcher, I. White, F.C. Walsh and J.P. Millington, *J. Appl. Electrochem.* **21** (1991) 667.
10. M. Abda, Z. Gaura and Y. Oren, *J. Appl. Electrochem.* **21** (1991) 734.
11. C. Ponce de Leon and D. Pletcher, *Electrochim. Acta* **41** (1996) 533.
12. R.C. Widner, M.F.B. Sousa and R. Bertazzoli, *J. Appl. Electrochem.* **28** (1998) 201.
13. D.R. Gabe, 'Principles of Metal Surface Treatment and Protection' 2nd edn (Pergamon Press, Oxford, 1978).
14. R. Suzuki, W.-H. Li and K. Nobe, *Plat. Surf. Finish.* **12** (1995) 58.
15. J. St-Pierre, N. Massé, É. Fréchette and M. Bergeron, *J. Appl. Electrochem.* **26** (1996) 369.

16. Water Regulations Act (US) (1989), Landesamt Fur Wasser Und Abfall (DL) (1982) and Conselho Nacional do Meio Ambiente (BR) (1986).
17. J. Wang, *Electrochim. Acta* **26** (1981) 1721.
18. T. Hurlen and K.P. Fischer, *Electroanal. Chem. & Interf. Electrochem.* **61** (1975) 165.
19. A.R. Despic and M.G. Pavlovic, *Electrochim. Acta* **27** (1982) 1539.
20. J. McBreen and E. Gannon, *J. Electrochem. Soc.* **130** (1983) 1667.
21. A.C. Beshore, B.J. Flori, G. Schade and T.J. O'Keefe, *J.Appl. Electrochem.* **17** (1987) 765.
22. J. St-Pierre and D.L. Piron, *J. Electrochem. Soc.* **139** (1992) 105.
23. I. Epelboin, M. Ksouri and R. Wiart, *J. Electrochem. Soc.* **122** (1975) 1206.
24. I. Epelboin, M. Ksouri and R. Wiart, *Faraday Symp. Chem. Soc.* **12** (1978) 115.
25. I. Epelboin, M. Ksouri and R. Wiart, *J. Electroanal. Chem.* **65** (1975) 373.
26. M.D. Pritzker and T.Z. Fahidy, *J. Electrochem. Soc.* **136** (1989) 2238.
27. A.T.S. Walker and A.A. Wragg, *Electrochim. Acta* **22** (1977) 1129.
28. S. Person, *Polymer* **29**(5) (1988) 802.
29. C.D. Iacovangelo and F.G. Will, *J. Electrochem. Soc.* **132** (1985) 851.
30. D.J. Pickett, 'Electrochemical Reactor Design' (Elsevier Scientific, New York, 1979).
31. A. Storck, M.A. Enriquez-Granados and M. Roger, *Electrochim. Acta* **27** (1982) 293.
32. T. Doherty, J.G. Sunderland, E.P.L. Roberts and D.J. Pickett, *Electrochim. Acta* **41** (1996) 519.